Journal of Solar Energy Research (JSER)

Journal homepage: www.jser.ut.ac.ir

A Distributed Control Strategy for Load Sharing and Harmonic Compensation in Islanded PV-based Microgrids

Morteza Haghshenas[a,*]

[a] *Department of Electrical Engineering, University of Isfahan, P.O. Box: 81746-73441, Isfahan, Iran.*

ARTICLE INFO

Article Type:

Research Article

Received:26.01.2024
Accepted:15.09.2024

Keywords:
Distributed control,
Harmonic compensation,
Nonlinear load sharing,
PV-based microgrid,
PV inverter.

A B S T R A C T

In recent years, the use of photovoltaic (PV) systems has grown significantly in distribution systems and microgrids (MGs). The PV systems are connected to the MG through an interface inverter. However, when multiple PV inverters are paralleled in a MG, load sharing among PV inverters and their coordinated control to compensate for voltage disturbances become critical challenges. This paper proposes a novel control strategy to guarantee power quality in PV-based islanded MGs. In the proposed strategy, each PV system has a primary control level and a secondary control level. The primary control level of PVs consists of fundamental and harmonic virtual impedance loops that improve fundamental power sharing and distortion power sharing among PV inverters, respectively. In the proposed strategy, the secondary control levels along with the primary controllers are implemented locally to reduce disturbances in the communication system. This control level includes voltage and frequency restoration units and a harmonic compensation unit that generates appropriate control signals and directs the compensation of voltage disturbances in the MG load bus. The simulation results have confirmed the effectiveness of the proposed strategy for fundamental and non-fundamental power sharing among PVs and increasing power quality in islanded MGs with different resource capacities.

1. Introduction

With increasing concern about the environment, the inclusion of PV-based microgrids in the contemporary energy sector has become more common. Microgrids are small-scale power systems consisting of distributed generators (DGs), energy storage systems, and interconnected loads that can operate in both grid-connected and islanded modes [1]. In an islanded MG (IMG), the PVs must control the output power independently to avoid overload and ensure that the voltage and frequency vary within an acceptable range [2]. Accordingly, hierarchical control schemes are presented to provide active and

*Corresponding Author Email:haghshenas.research@gmail.com

Cite this article: Haghshenas, M. (2024). A Distributed Control Strategy for Load Sharing and Harmonic Compensation in Islanded PV-based Microgrids. Journal of Solar Energy Research, 9(2), 1926-1941. doi: 10.22059/jser.2024.371687.1377

DOI: 10.22059/jser.2024.371687.1377

reactive power control and integrate basic capabilities with more advanced capabilities such as voltage and frequency regulation [3]. The hierarchical structures for IMGs consist of primary and secondary control levels. The primary control level includes DG local controllers and the secondary control level recovers the voltage and frequency of the DGs output [4]. In the hierarchical control strategy, the secondary control level acts as a central controller [5], [6], [7]. Among the existing approaches, droop control has been frequently applied in control structures [8], [9], [10], [11]. By considering typical P-F and Q-V droops, the active power can be accurately shared because the frequency is uniform in the steady state, and reactive power sharing is more challenging because the voltage is non-uniform [12]. However, the main challenge of droop-based approaches is to balance the precision of power sharing and regulation of voltage amplitude and frequency, as well as to reduce power fluctuations among DGs [4]. To cope with this problem, improvements in droop control have been proposed, such as using virtual impedance [13], [14], [15].

On the other hand, with the increase of nonlinear loads, the power quality of MGs becomes prominent. In IMGs, power quality requires more attention, because the short-circuit ratio is much lower than in traditional power systems [16]. With recent advances in power electronics, the multifunctional inverter used to connect DGs to MGs plays an important role in ensuring and improving power quality. A decentralized control scheme was proposed in [10] for compensating voltage harmonics based on creating a resistive behavior at harmonic frequencies. Wang et al. [17] have proposed a decentralized control strategy for IMGs, in which a load compensator is used apart from the use of droop controllers and internal voltage and current control loops. Hosseinpour et al. [18] have proposed a method called capacitor-current proportional-integral positive active damping to mitigate the resonance caused by the LCL filter in a grid-connected PV power conditioning system. Zhou et al. [19] have proposed a decentralized adaptive control technique for reactive and distortion power sharing in a consensus protocol. Gao and Ai [20] have also presented a study using a consensus approach to improve active and reactive power flow in MGs by applying multi-objective scheduling optimization. Both method presented in [19] and [20] have used droop control principles and require communication among neighboring DGs, but do not rely on a central controller. Sreekumar et al. [21] have introduced a different approach by combining variable virtual impedance and feed-forward control to achieve uniform harmonic sharing without the need for communication. This concept utilizes the capability of DGs without exceeding their maximum current. Guerrero et al. [22] have proposed a hierarchical approach that includes a secondary controller with a communication link. This approach allows active and reactive power sharing, but does not support distortion power sharing among DGs. In the mentioned methods, compensation of voltage harmonics has been done at the output point of DGs. While in IMGs, the power quality in the load bus is very important. Furthermore, while DGs try to compensate voltage harmonics locally at their output, harmonic distortion may increase at other buses such as the sensitive load bus (SLB).

According to the findings of [23] and [24], any failure in the communication link that connects the primary control level and the MG central controller (MGCC) can disrupt the operation of the control system in an IMG. To address communication security concerns, several decentralized secondary approaches have been proposed in previous works [8], [9], [10], [12], [17], [19], [25]. The approach proposed in [26] prioritizes frequency control and allocates power sharing. Similarly, Ibacache et al. [27] have presented a decentralized unified secondary frequency control technique that includes voltage constraints in MGs. However, these approaches lack thorough theoretical analysis, raising doubts as to whether they can effectively achieve their intended goals. Gu et al. [28] have proposed a decentralized controller based on a nonlinear state estimator for MG voltage restoration. However, the nonlinear estimation technique is complex and cannot be applied to frequency restoration. Khayat et al. [29] have solved the secondary frequency control problem in MGs using a decentralized linear quadratic regulator. Although it effectively mitigates the frequency deviation, it does not maintain the desired power sharing ratio.

In this paper, we propose a distributed secondary control structure for non-fundamental (harmonic) power sharing and harmonic compensation in IMGs, inspired by the previous discussions. In the proposed approach, the communication link between the primary controllers and MGCC is excluded, and instead, a local secondary controller is taken into account for each DG. The key contributions of this paper are as follows:

- An efficient framework for virtual impedances is proposed, which combines additional harmonic virtual impedance loops alongside virtual

fundamental impedance to increase the accuracy of harmonic power sharing among PVs.

- The implementation of secondary controllers of PVs in a decentralized manner, without relying on MGCC, has increased the reliability of the MG control system.
- Instead of compensating the voltage harmonics in the inverter output, PVs try to compensate the voltage harmonics in the MG sensitive load bus.
- Harmonic compensation workload sharing among PVs is determined based on the available free capacity of their inverters.

The remainder of this paper is organized as follows: the proposed control scheme is explained in section 2. Sections 3 and 4 consists of the simulation results and their comparison with other existing methods, respectively. Finally, the key findings of the paper have been concluded in section 5.

2. Proposed Control Scheme

The proposed control scheme and its implementation in an IMG is shown in Figure 1. The MG consists of several DGs (PVs) connected to the PV bus through a voltage source inverter (VSI) and distribution lines. Linear and non-linear loads are connected to the sensitive load bus. Notably, each PV has two levels of control: primary and secondary. Both levels are implemented locally and are adjacent to each other. Importantly, there is no communication link between primary and secondary control levels. Secondary controllers generate control signals based on PV output measurements and SLB parameters.

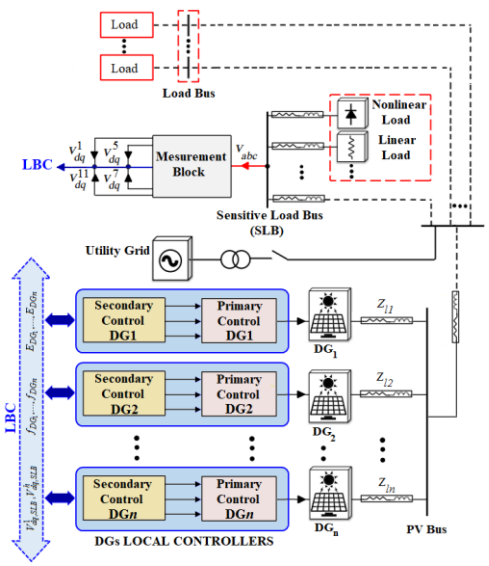

Figure 1. The proposed control scheme based on distributed secondary control (DSC).

The primary control level includes droop controllers, voltage and current controllers, and virtual impedance loops. The secondary control is distributed and consists of applying reference signals to the primary controller to adjust the PV voltage and frequency and compensate for SLB voltage harmonics. Since there may be a long distance between the SLB and the PV bus, the SLB voltage parameters are transmitted to the secondary controllers using low-band communication. Low-band communication is chosen to ensure that the transmitted data is close to DC signals. As a result, the fundamental and harmonic components of the SLB voltages are extracted in the synchronous reference frame (dq) and then sent to the secondary controllers. Note that this paper focuses on compensating the 5th, 7th, and 11th voltage harmonics as primary harmonics. The extraction process for the fundamental and harmonic components of the SLB voltage can be found in the "Measurement block" shown in Figure 2. In addition, Sections 2.1 and 2.2 provide details on the proposed primary and secondary control levels, respectively.

2.1. Proposed PVs Primary Controllers

The structure of the PV_K power stage and the details of its primary and secondary control levels are shown in Figure 2. The PV power stage consists of a DC prime mover vdc, an interface inverter and an LCL filter. It is worth noting that this paper focuses on control of PV inverter. Therefore, it is assumed that a nearly constant DC voltage is supplied in the DC link. However, a feed-forward loop is considered to compensate for possible *vdc* variations and generate gate signals using a pulse width modulation (PWM) block. The proposed control scheme is designed in a stationary reference frame ($\alpha\beta$) and the Clark transform is used to transform the parameters [30]. As shown in the primary control block of PV_k (see Figure 2), the output voltage reference of PV is generated in the $\alpha\beta$ frame ($v^*_{\alpha\beta}$) by droop characteristics, virtual impedance loops, and SLB voltage harmonics compensation reference (v^*c). On the other hand, the instantaneous voltage of the inverter's output filter (vo_{abc}) is transformed into $\alpha\beta$ reference frame, and after comparison with $v^*_{\alpha\beta}$, generates the current control reference ($i^*_{\alpha\beta}$). Finally, the response of the current controller to the error resulting from the comparison of the output filter inductor current and $i^*_{\alpha\beta}$ is given back to the ABC

frame to generate the three-phase reference voltages, and the PWM block controls the inverter based on this reference.

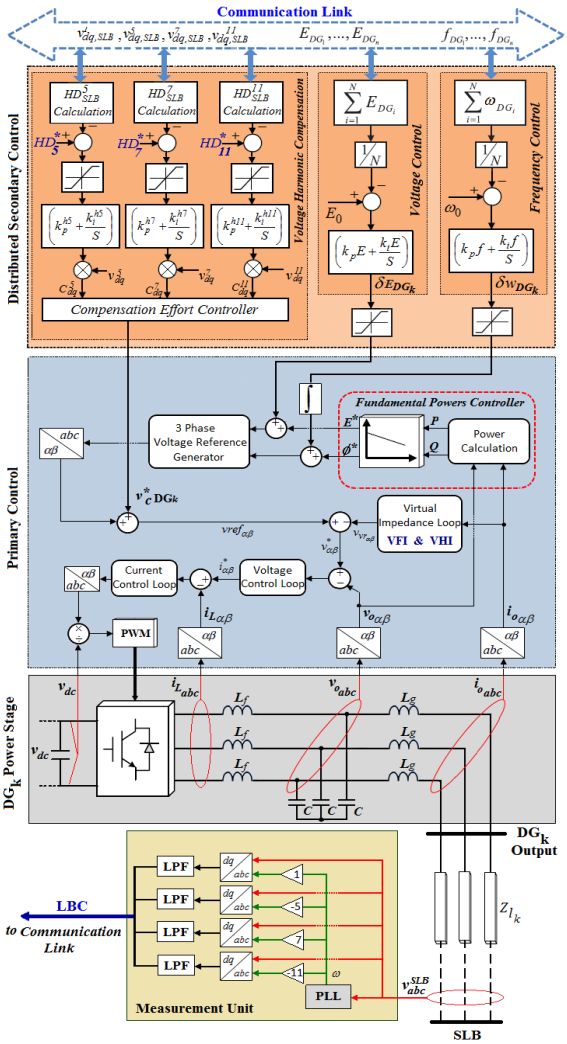

Figure 2. The proposed primary and secondary controllers.

2.1.1. Fundamental Power Controllers

As shown in Figure 2, to calculate the instantaneous active and reactive powers, $vo_{\alpha\beta}$ and $io_{\alpha\beta}$ are applied to the "power calculation" block in which the instantaneous active and reactive powers are calculated as follows [5]:

$$p = \bar{p} + \tilde{p} = v_\alpha i_\alpha + v_\beta i_\beta \quad (1)$$

$$q = \bar{q} + \tilde{q} = v_\beta i_\alpha - v_\alpha i_\beta \quad (2)$$

Instantaneous active and reactive power are calculated by (1) and (2), which have a DC component and a distortion component. The distortion component is created due to the presence of voltage and current harmonics. The DC components can be extracted using low-pass filters. This paper used first-order filters with a cutoff frequency of 2 Hz to separate these components. In an electrical system consisting mainly of inductive impedances, the fundamental active and reactive powers can be controlled independently. This is achieved by adjusting the phase angle and amplitude of the output voltage of the PVs. Therefore, Q-E and P-ω droop characteristics have been used to share fundamental power among PVs in an IMG [30].

$$\phi^* = \phi_0 - (m_p.\bar{p} + \frac{m_i}{s}.\bar{p}) \quad (3)$$

$$E^* = E_o - n_p.\bar{q} \quad (4)$$

Where ϕ^* is the phase angle reference, E^* is the voltage amplitude reference, $\bar{p}$ and $\bar{q}$ are fundamental active and reactive powers, ϕ_o is the rated value for voltage phase angle, E_o is the rated value for voltage amplitude, m_p and m_i are the proportional and integral coefficients of active power controller, and n_p is the proportional coefficient of reactive power controller.

2.1.2. Voltage and Current Control Loops

Since PI controllers do not perform well in controlling non-DC variables, it is preferable to use proportional resonant (PR) controllers in the $\alpha\beta$ reference frame. In the proposed scheme, voltage and current controllers are implemented as follows [6]:

$$G_V(s) = k_{pV} + \sum_{h=1,5,7,11} \frac{2.k_{rV_h}.\omega_{cV}.S}{S^2 + 2.\omega_{cV}.S + (h.\omega_0)^2} \quad (5)$$

$$G_I(s) = k_{pI} + \sum_{h=1,5,7,11} \frac{2.k_{rI_h}.\omega_{cI}.S}{S^2 + 2.\omega_{cI}.S + (h.\omega_0)^2} \quad (6)$$

Where k_{pV} and k_{pI} are voltage and current proportional coefficients, respectively, k_{rVh} and k_{rIh} are resonant coefficients for h^{th} harmonic order, and ω_c is the cut-off frequency of the PR controller.

2.1.3. Proposed Virtual Impedance Loops

In IMGs, the impedance of the distribution line has a significant impact on the accuracy of power-sharing among PV units. Therefore, by creating a proper virtual impedance at the fundamental frequency, the amplitude and phase angle of the output impedance of PVs can be set in a way that the effect of the asymmetry of the line impedances on the accuracy of power-sharing among PVs is minimized. Virtual resistance makes the oscillations of the system more damped, and the virtual inductance at the fundamental frequency can make the PV output impedance more inductive, and as a result, it can improve the performance of droop controllers.

Therefore, in this paper, a virtual fundamental impedance (VFI) loop consisting of a resistance and a positive inductance is used as the base structure of virtual impedance. The base structure of virtual impedance has been developed in [7] and [31] for creating a virtual impedance at harmonic frequencies and as a result, improving the nonlinear load sharing among PVs. In the system studied in [7] which is a grid-connected MG, LC filters have been used in PV output. While, in the approach proposed in this paper (see Figure 2), an output inductor (L_g) is also used to decrease the circulating harmonic currents among PVs and to improve the performance of the fundamental power controllers. If the voltage and current controllers are designed properly, the disturbance of the LC filter's output voltage (vo_{abc}) can be limited. However, there will still be a harmonic voltage drop across L_g which creates voltage distortion at the PV output. Since the MG's loads are located nearby, this disturbance has the potential to impact the performance of sensitive loads.

This paper proposes in addition to VFIs, the virtual harmonic impedance (VHI) loops should be implemented to address the issue of harmonic voltage drop across the L_g. The proposed VHIs consist of a positive resistance and a negative inductance (capacitive) to compensate for these harmonics. In the VHIs, the presence of virtual harmonic resistance enhances the load sharing capabilities among PVs, while the capacitive virtual inductance counteracts the undesirable effects of PV's output inductor to harmonic frequencies. Additionally, the VFIs compensate for the asymmetrical effects of distribution lines and create suitable conditions for the effective operation of fundamental power controllers. VFI and VHI loops are implemented based on the (7) and (8), in which ω_0 is the fundamental frequency, R_v and L_v are virtual resistance and inductance, respectively. The fundamental and harmonic components of PV output current (i_o) are separated as follows:

$$\begin{bmatrix} V_{v\alpha}^{1} \\ V_{v\beta}^{1} \end{bmatrix} = \begin{bmatrix} R_v^1 & -\omega_0.L_v^1 \\ \omega_0.L_v^1 & R_v^1 \end{bmatrix} . \begin{bmatrix} i_{o\alpha}^{1} \\ i_{o\beta}^{1} \end{bmatrix} \quad (7)$$

$$\begin{bmatrix} V_{v\alpha}^{h} \\ V_{v\beta}^{h} \end{bmatrix} = \begin{bmatrix} R_v^h & h.\omega_0.L_v^h \\ -h.\omega_0.L_v^h & R_v^h \end{bmatrix} . \begin{bmatrix} i_{o\alpha}^{h} \\ i_{o\beta}^{h} \end{bmatrix} \quad (8)$$

It is noted that, in the design of the VFI loops, an increase of R^h_v for improving nonlinear load sharing causes PV's output voltage to be disturbed due to harmonic drop voltage on R^h_v. Thus, a compromise should be created between PV's output disturbance and the accuracy of nonlinear load sharing in selecting the VFI loop's parameters. Worth noting that VHI loops should just be put on the path of main harmonic currents to maintain the L_g's desirable effects in limiting the circulating current and also in keeping the mostly inductive impedance of MG in the fundamental component. Figure 3 illustrates how the proposed virtual impedances impact both the fundamental and harmonic frequencies. In the figure, V_o' and Z_o' are the voltage and output impedance of the inverter which has an LC filter without the presence of virtual impedance, respectively. In addition, V_O is the output voltage of the LC filter by the presence of virtual impedance and V_{Out} is the output voltage of the LCL filter.

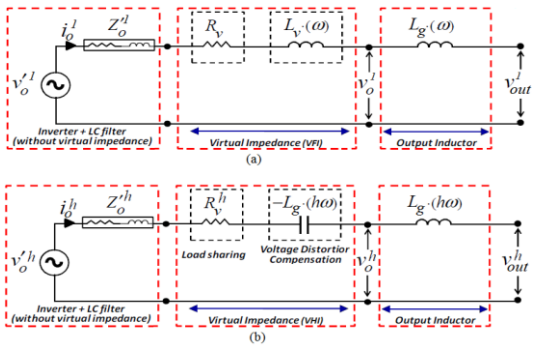

Figure 3. The equivalent circuit of inverter at fundamental (a) and harmonic (b) frequencies.

2.1.4. Primary Controller Design

This paper examines an IMG that includes three PVs, where PV_1 has a power rating twice as high as PV_2 and PV_3 ($S0_1$=2$S0_2$=2$S0_3$). Therefore, the parameters of PV_1 can be determined by stability analysis and the parameters of other units can be adjusted based on their capacity. However, stability analysis can also be carried out for PV_2 and PV_3 and similar results can be obtained. In this regard, the approach for designing the droop characteristics of power control is sufficiently discussed in [22] and [30], so it will not be mentioned here. The local control system and the power stage of PV can be modeled as follows:

$$V_o(s) = G_{cl}(s).V_{ref}(s) - Z_o(s).I_o(s) \quad (9)$$

Where $V_{ref}(s)$, $G_{cl}(s)$ and $Z_o(s)$ are the reference voltage, control system closed-loop transfer function, and output impedance, respectively. $G_{cl}(s)$ and $Z_o(s)$ can be expressed as (10) and (11), respectively.

$$G_{cl}(s) = \left.\frac{V_o(s)}{V_{ref}(s)}\right|_{Io(s)=0} = \frac{G_v(s).G_d(s).G_I(s)}{LCs^2 + (r_L + G_I(s).G_d(s)).Cs + G_v(s).G_d(s).G_I(s)} \quad (10)$$

$$Z_o(s)=\frac{V_o(s)}{I_o(s)}\bigg|_{Vref(s)=0}=Z'_o(s)+Z_v(s) \quad (11)$$

Where r_L is the filter inductor resistance, *Gd(s)* is the PWM transfer function, and *Zv(s)* represents the fundamental virtual impedance. The inverter output impedance can be determined as follows:

$$Z'_o(s)=\frac{Ls+r_L+G_I(s).G_d(s)}{LCs^2+(r_L+G_I(s).G_d(s)).Cs+G_v(s).G_d(s).G_I(s)} \quad (12)$$

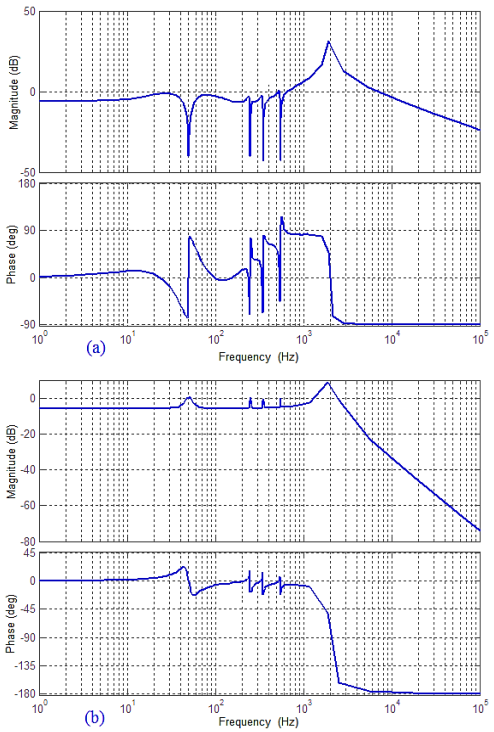

Figure 4. Bode diagrams for inverter output impedance (a) and closed loop control system (b).

The parameters listed in Table 1 are considered for the proposed virtual impedances. According to the PV's power stage parameters mentioned in Table 3, the impedance phase angle of PV_1 is equal to 77 degrees and the corresponding values for PV_2 and PV_3 are calculated to be about 75 degrees. Therefore, the mainly inductive electrical system considered in this paper for active and reactive power control is obtained using the parameters listed in Table 1. According to (10) and (12), the Bode diagrams shown in Figure 4 are obtained for the output impedance of the inverter and the closed-loop transfer function. As shown in Figure 4(a), the output impedance of the inverter is almost negligible at the fundamental and harmonic frequencies. This shows that the proposed virtual impedances are effective in achieving the desired output impedance of the inverter. In addition, Figure 4(b) shows that the gain and phase angle of the closed-loop transfer function are equal to 1 and 0, respectively, at the mentioned frequencies. The results show that the reference voltage is accurately tracked.

2.2. Proposed PVs Secondary Controllers

The details of the proposed secondary controller for each PV are shown in Figure 2. The proposed secondary controller consists of three units: frequency restoration, voltage restoration, and SLB voltage harmonics compensation.

2.2.1. Distributed Frequency Control

To address the frequency deviation caused by local P-ω droop controllers in MGs, secondary frequency controllers are proposed. However, this approach requires communication to avoid instability in the MG, which is likely due to variations in local inverters. The proposed secondary control strategy involves measuring the frequency of each PV at regular intervals, transmitting it to other PVs, calculating the average frequency measured by other PVs, and then adjusting the frequency as follows [23]:

$$\delta\omega_{PV_k}=k_{pf}(\omega_0-\bar{\omega}_{PV_k})+k_{if}\int(\omega_0-\bar{\omega}_{PV_k})dt$$
$$\bar{\omega}_{PV_k}=\frac{\sum_{i=1}^{N}\omega_{PV_i}}{N} \quad (13)$$

Where ω_0 denotes the fundamental frequency, $\bar{\omega}_{PV_k}$ represents the frequency average for all PV units, and $\delta\omega_{PV_k}$ indicates the control signal generated by the secondary control of PV_k at each sample time. Here, i=1,2,…,N , k=1,2,…,n , N is the number of packages (frequency measurements) arrived through communication system and n is number of PV units. Figure 5 illustrates how the secondary controller addresses frequency and voltage deviation caused by the primary control level in the MG. The figure also illustrates that the secondary control simply adjusts the primary response to ensure that the frequency reaches the rated value, regardless of the power rates of the PVs. However, it is important to mention that the power change needed for the proposed DSC utilizing the average technique is influenced by the power rates of the PVs.

2.2.2. Distributed Voltage Control

A similar technique that reflects the distributed frequency control approach can be used. In the proposed technique, each inverter monitors the

voltage error and tries to correct the voltage deviation caused by the Q-E droop. This technique offers an advantage over the traditional method that remote sensing, which is used in the central secondary control, is not necessary. Only the voltage of each PV terminal, which may differ significantly from the other terminals, is required. In this manner, voltage restoration is achieved in the following manner [23]:

$$\delta E_{PV_k} = k_{pE}(E_0 - \bar{E}_{PV_k}) + k_{iE}\int (E_0 - \bar{E}_{PV_k})dt$$
$$\bar{E}_{PV_k} = \frac{\sum_{i=1}^{N} E_{PV_k}}{N} \quad (14)$$

Where δE_{PV_k} is the restoration voltage signal of PV$_k$ and produced by using the PI control of the error between voltage reference (E_0) and average voltage ampelitude of PV units ($\bar{E}_{PV_k}$) in every sample time. According to the proposed average technique, secondary control can remove voltage deviations caused by the primary control level in every PV unit, as illustrated in Figure 5(b).

A small signal model block diagram for frequency and voltage controllers is shown in Figure 6. This model consists of two components: droop control model and distributed secondary control model. In the droop control model, a low-pass filter is used to calculate the power. On the other hand, the secondary control model uses a simple phase-locked loop (PLL) with a first-order transfer function (GPLL(s)) to extract the PV output frequency/voltage [30]. It also has a proportional gain (ka) to align the average frequency/voltage with measurements from other PVs and a PI controller (Gsec(s)).

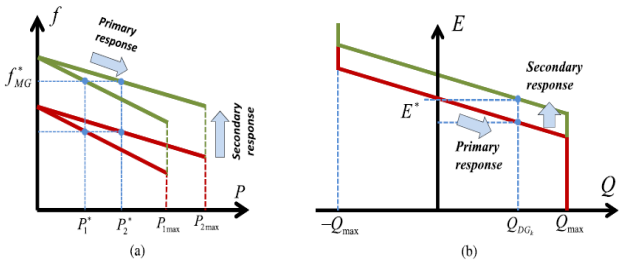

Figure 5. Secondary control response; frequency restoration (a), voltage restoration (b).

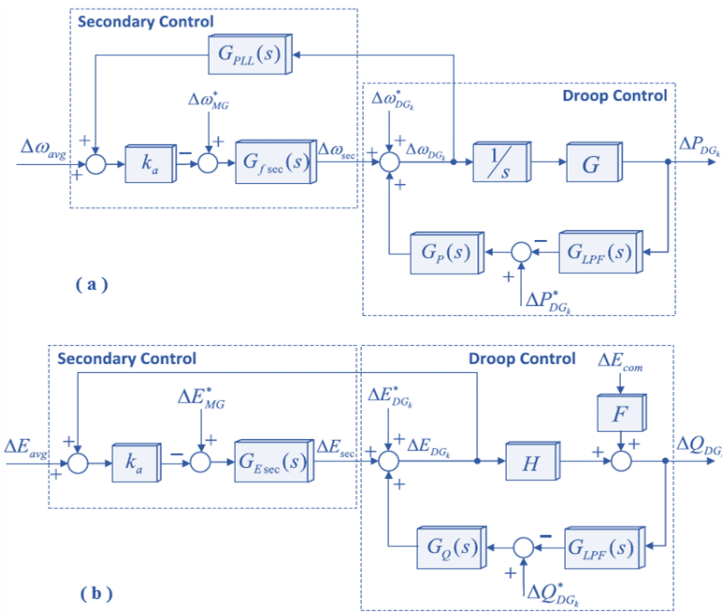

Figure 6. Small signal models of distributed frequency (a) and voltage (b) control for a PV unit in an inductive IMG.

2.2.3. Voltage Harmonics Compensator

The voltage harmonics compensator operates differently compared to the voltage and frequency control units in the microgrid. While the voltage and frequency control units work based on the average output voltage and frequency of all PVs, the harmonics compensator specifically focuses on compensating for harmonics in the sampled parameters of the SLB. As shown in Figure 2, the

fundamental and harmonic components of SLB voltage are separated in the "Measurement block" and transmitted to the communication system. Next, in the "voltage harmonics compensator" block, a harmonic distortion index (HD^h_{SLB}) is calculated for specific harmonics using (15). Following this, the HD^5_{SLB}, HD^7_{SLB}, and HD^{11}_{SLB} values are compared to reference values (HD^*_5, HD^*_7 and HD^*_{11}), respectively. The resulting errors are then used to adjust the PI controllers. The output from the PI controllers is multiplied by v^5_{dq}, v^7_{dq}, and v^{11}_{dq}, resulting in the computation of C^5_{dq}, C^7_{dq}, and C^{11}_{dq}.

$$HD^h_{SLB} = \frac{\sqrt{(v^h_d)^2 + (v^h_q)^2}}{\sqrt{(v^1_d)^2 + (v^1_q)^2}}.100 \qquad (15)$$

The proposed control strategy includes a compensation effort controller that is responsible for sharing the compensation workload among PVs. Figure 7 shows the block diagram of this controller, where S_0, S_{fr}, and S_r represent the rated capacity of PV, the available capacity for supplying non-fundamental power, and the remaining capacity after supplying non-fundamental power, respectively. The calculation method for determining S_{fr} is presented in Figure 7. This figure also defines S_f and S_n as apparent powers for fundamental and non-fundamental powers. The total power supplied by each PV unit (S) can be calculated as follows [32]:

$$S = \sqrt{(S_f)^2 + (S_n)^2} \qquad (16)$$

The performance of the "Droop characteristic" (see Figure 7) is stated as follows [32]:

$$C^h_{dq,k} = \begin{cases} C^h_{dq}.(S_{fr} - S_n) & S_r > 0 \\ 0 & S_r \le 0 \end{cases} \qquad (17)$$

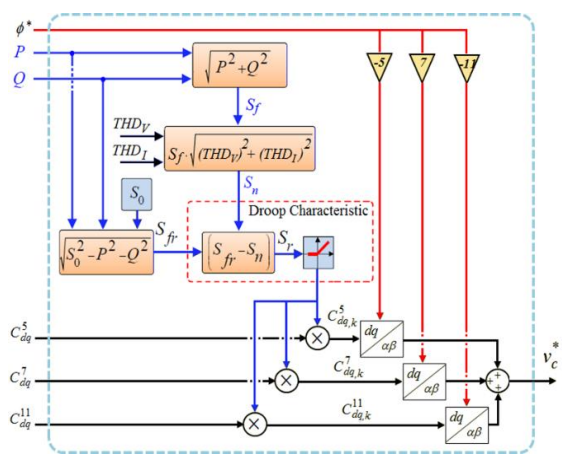

Figure 7. Block diagram of compensation effort controller in the proposed control scheme.

According to (17), if S_r>0 (while not exceeding the rated capacity of PV), the value of $C^h_{dq,k}$ will decrease as S_n increases. This decrease in $C^h_{dq,k}$ indicates that the compensation effort of PV_k is reduced. In other words, there is an inherent negative feedback in the proposed compensation method that promotes nonlinear load sharing among PVs. This phenomenon is also evident in the simulation results. Once the compensation reference for the h^{th} harmonic (C^h_{dq}) is multiplied by S_r, the compensation signal for this harmonic in PV_k ($C^h_{dq,k}$) is generated. Afterward, the compensation references for the primary harmonics are combined in a stationary reference frame, resulting in the generation of the total reference for compensating SLB voltage harmonics (v^*c).

3. Simulation Results

The IMG shown in Figure 8 is considered as the test system. It consists of three PVs with a power stage and the control system shown in Figure 2. The power stage and control system parameters can be found in Tables 1-3. MATLAB/SIMULINK is used to perform simulations with SIM Power Systems Toolbox. The rated voltage and frequency of MG are set to 230V and 50Hz, and the PV inverters have a switching frequency of 10kHz. Figure 8 shows the presence of the diode rectifier as a non-linear load along with a star-connected linear load (ZL) connected to the SLB. Zl represents the distribution lines between PV and SLB. Table 3 provides data on the impedance of distribution lines that are unequal. This unequal impedance condition highlights the role of VHI loops in improving nonlinear load sharing accuracy.

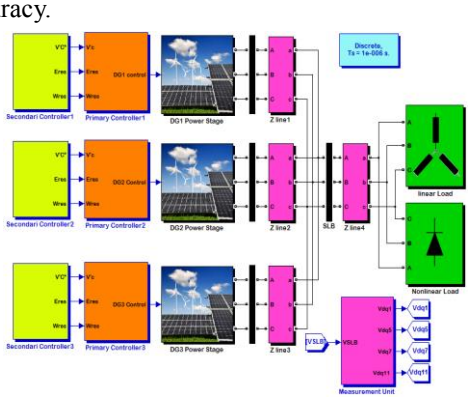

Figure 8. The structure of the IMG simulated in MATLAB/SIMULINK.

Table 1. PVs primary controller parameters.

Droop characteristics of fundamental power controllers	
PV1	PV2 , PV3

m_p (rad/W)	m_i (rad/W.s)	n_p (V/VAR)	m_p (rad/W)	m_i (rad/W.s)	n_p (V/VAR)
$8*10^{-6}$	$8*10^{-5}$	$8*10^{-2}$	$16*10^{-6}$	$16*10^{-5}$	$16*10^{-2}$
Voltage control loops (PV1, PV2, PV3)					
k_{pV}	k_{rV1}	k_{rV5}	k_{rV7}	k_{rV11}	ω_{cV} (r/s)
1	105	105	150	150	1
Current control loops (PV1, PV2, PV3)					
K_{IV}	k_{rI1}	k_{rI5}	k_{rI7}	k_{rI11}	ω_{cI} (r/s)
5	400	110	110	110	1
Fundamental and Harmonics virtual impedance loops					
PV1			PV2 , PV3		
$L_{V,l}$ (mH)	$R_{V,l}$ (Ω)	$L_{V,h}$ (mH)	$R_{V,h}$ (Ω)	$L_{V,l}$ (mH)	$R_{V,l}$ (Ω)	$L_{V,h}$ (mH)	$R_{V,h}$ (Ω)
0.25	3	16.812	-1.8	0.5	6	7.074	-1.8

To evaluate the effectiveness of the proposed control strategy in power sharing among PVs and voltage harmonic compensation, simulation results are presented in a series of four steps. Step 1 ($0 < t < 1.5$) demonstrates the outcomes of the local control of PVs using the basic control structure, without any compensation for enhancing power quality. Step 2 ($1.5 < t < 3$) investigates the impact of the VHI loops on system performance after incorporating them into the basic control structure. Step 3 ($3 < t < 4.5$) activates the secondary controllers, which transmit voltage and frequency restoration signals, as well as SLB voltage harmonics compensation signals, to the primary controllers. Finally, in the fourth step ($4.5 < t < 6$), the secondary controller of PV3 is completely deactivated to evaluate the behavior of the system under a fault condition.

Table 2. PVs secondary controller parameters.

Distributed voltage and frequency controllers			
K_{pf}	K_{if}	K_{pE}	K_{iE}
0.025	0.15	0.247	0.203
SLB voltage harmonics compensator units					
K_{p5}	K_{i5}	K_{p7}	K_{i7}	K_{p11}	K_{i11}
0.617	18.304	0.617	18.642	0.617	13.517

Table 3. MG power stage parameters.

PVs power stage parameters						
Vdc (V)		Cf (μF)	Lf (mH)		Lg (mH)	
650		25	1.2		1.2	
Distribution lines (*Zl*)			Nonlinear load			Linear load
PV1 (Ω)	PV 2,3 (Ω)	Load (Ω)	R_{NL} (Ω)	L_{NL} (mH)	C_{NL} (μF)	Z_L (Ω)
0.2+j0.8	0.08+j0.4	0.05+j0.08	50	0.08	200	50+j6.5

To evaluate the effectiveness of the proposed control strategy in power sharing among PVs and voltage harmonic compensation, simulation results are presented in a series of four steps. Step 1 ($0 < t < 1.5$) shows the results of local control of PVs using the basic control structure, without any compensation to increase the power quality. Step 2 ($1.5 < t < 3$) examines the effect of VHI loops on system performance after incorporating them into the main control structure. Step 3 ($3 < t < 4.5$) activates the secondary controllers, which send voltage and frequency restoration signals as well as SLB voltage harmonics compensation signals to the primary controllers. Finally, in the fourth step ($4.5 < t < 6$), the secondary controller PV_3 is completely disabled to evaluate the behavior of the system under fault conditions.

3.1. Step 1 ($0 < t < 1.5$)

Figure 9 shows the output voltage of PVs and SLB and their harmonic spectrum in the first to fourth steps of simulation. As shown in Figure 9, in the first step, where the VHI loops are not yet activated, the output voltage of the PVs is almost sinusoidal. This can be seen from the low values of total harmonic distortion (THD) and harmonic distortion indices (*HD5*, *HD7* and *HD11*) presented in Figure 9.

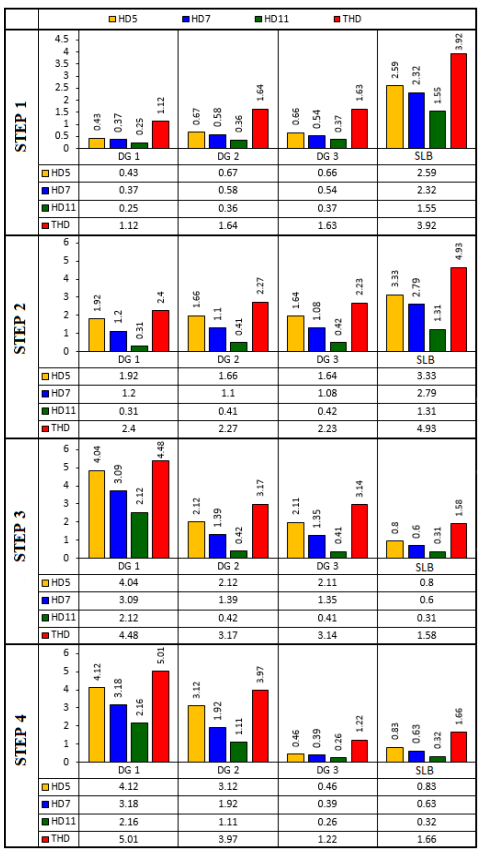

Figure 9. Voltage harmonic indices in the simulation steps 1-4.

The results from the first step of simulation show that the voltage controllers effectively follow the reference generated by the droop characteristics.

Although the output voltages of the PVs remain sinusoidal in this step, the SLB voltages show significant distortion, as evident in Figure 9. The main cause of this distortion is the harmonic voltage drop in the distribution lines. Although the output voltage of PVs is close to sinusoidal, the presence of this impedance causes disturbances in the SLB voltage. Figure 10 shows the changes of different power components in the simulation periods. As shown in Figures 10(a) and 10(b), despite the asymmetry in the impedance of the distribution lines, the fundamental active and reactive powers are correctly divided. Therefore, the simulation results show the accurate performance of the VFI loops and confirm the proper performance of the droop characteristics in controlling the fundamental powers. But, from Figure 10(c), it can be seen that in the first step, the non-fundamental powers (*Sn*) are shared in the inverse ratio of the line impedances. While $S_{01}=2S_{02} = 2S_{03}$ and it was expected that the participation of PV_1 in providing non-linear load would be higher. Here, the non-fundamental power is calculated according to [32] and the details of THD calculation can be found in [30].

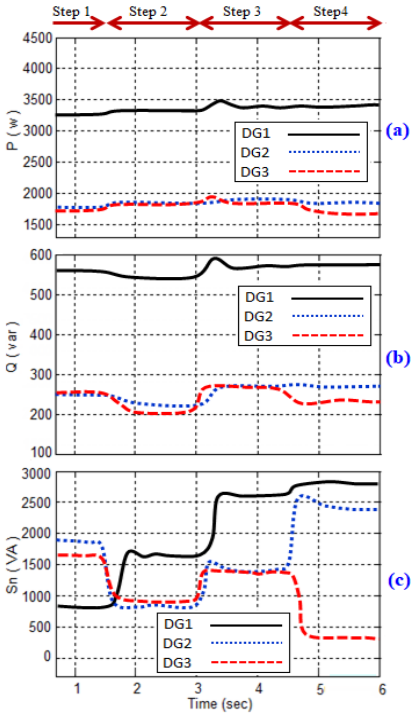

Figure 10. The fundamental active powers (a), the fundamental reactive powers (b), and the non-fundamental powers (c).

3.2. Step 2 (1.5 < t < 3)

The second step involves the integration of VHIs into the control system of PVs to handle sharing of harmonic currents. VHIs are strategically placed along the main harmonic current path to enhance the harmonic current sharing between PVs. As shown in Figure 10(c), it is clear that the inclusion of VHIs at t=1.5 sec significantly improves the *Sn* share, although it is still not proportional to the rated powers of the PVs. On the contrary, as shown in Figure 9, the combination of VHIs at harmonic frequencies leads to an amplified distortion in the output voltage of the PVs, which in turn leads to an increase in the voltage distortion in the SLB. Enhancing nonlinear load sharing, as described in Section 2, leads to increased voltage distortion at the PV terminals. In addition, slight changes in the fundamental powers can be seen in Figures 10(a) and 10(b) when VHIs are introduced. This can be attributed to the non-linearity of the load.

3.3. Step 3 (3 < t < 4.5)

In the third step, the secondary controllers of the PVs are activated at t=3sec. The secondary controllers compensate the voltage harmonics and restore the output voltage and frequency of the PVs. This helps reduce voltage and frequency deviations caused by Q-E and P-ω droop characteristics. Figure 11 shows the changes of the output voltage ampelitude and the frequency of PVs. As can be seen in Figure 11, the activation of the secondary controllers in the third step reduces the frequency deviation and voltage amplitude in the SLB.

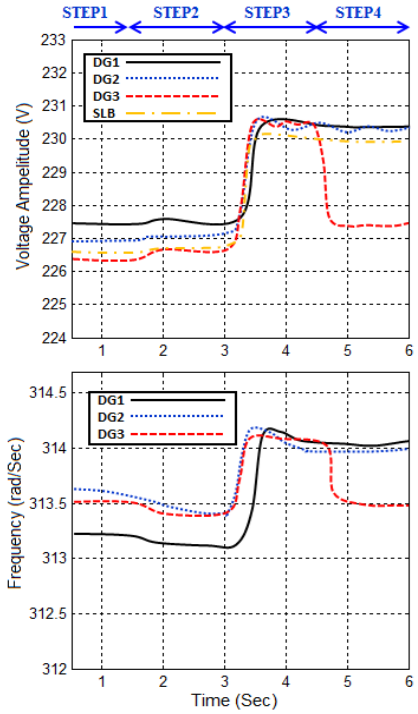

Figure 11. PVs output voltage and frequency in the simulation steps 1-4.

Figure 9 shows implementing SLB voltage harmonics compensation has significantly reduced the voltage harmonic indices at this specific point. However, the enhancement in SLB voltage quality comes at the expense of increased voltage distortion at the PVs output. This increase is necessary to ensure that a sinusoidal voltage is delivered at the SLB after accounting for the harmonic voltage drop along the distribution line and the VHIs. It should be emphasized that PV_1 supplies a larger amount of nonlinear load compared to the other units, due to its rated power and distribution line impedance. Figure 10(c) illustrates that after compensating for voltage harmonics through SLB, non-fundamental powers in all PVs are increased. This increase is primarily due to the greater increase in the currents of the main harmonics in PVs, enabling the compensation of voltage harmonics of the same order. Additionally, since PV_1 has a higher rated capacity compared to PV_2 and PV_3, it primarily supports the compensation of SLB voltage harmonics. Therefore, the results show a greater increase in non-fundamental power and voltage harmonic distortion in PV_1, when compared to other units. The improvement in nonlinear load sharing among PVs after compensating for SLB voltage harmonics is evident in Fig 10(c). It is observed that the nonlinear load is shared in proportion to the PVs rating capacity. This confirms the effectiveness of both the compensation effort controller and VHIs proposed in this paper.

3.4. Step 4 (4.5 < t < 6)

To evaluate the effectiveness of the proposed strategy when a part of the control system is disturbed, the secondary controller PV_3 was disabled at t=4.5 seconds. In this condition, PV_1 and PV_2 must compensate for SLB voltage harmonics and voltage and frequency regulation. As shown in Figure 9, disabling the secondary controller PV_3 resulted in a higher sinusoidal output voltage of PV_3 compared to the previous step. However, this increased the voltage distortion at the PV_1 and PV_2 outputs as they had to handle the compensating workload. This is evident from the high distortion indices for PV_1 and PV_2 in Figure 9. In addition, Figures 10(a) and 10(b) show that disabling the secondary controller PV_3 does not affect the primary power control and the primary controllers of the PVs operate independently of the secondary controller.

4. Comparison

This section examines the outcomes of comparing the proposed distributed secondary control strategy with decentralized [8], [9], [10], [12], [22], [26], [27] and central secondary control [5], [6], [7] strategies. To conduct this comparison, all strategies are deployed on the test system of Ref. [5]. Additionally, simulation results are compared in two main steps due to the absence of VHIs in Ref. [22]. In the first step (0sec<t<2.5sec), only the primary controllers of PVs are operational, and in the second step (2.5sec<t<5sec), the units responsible for enhancing power quality are activated. Regarding this matter, a droop characteristic is employed in [22] to share the harmonic power among PVs. In this method, H represents the non-fundamental power (Sn), while H_0 denotes the rated harmonic power. Accordingly, PV with higher rated power should possess a *G-H* droop characteristic with a shallower slope. This ensures that the compensation workload can be appropriately adjusted. Consequently, the values listed below have been chosen as the parameters for implementing the *G-H* droop characteristics in [22].

$$b_1 = -0.0005\ ,\ H_{0_1} = 2000$$
$$b_2 = -0.001\ ,\ H_{0_2} = 1000 \tag{18}$$

The simulation results for fundamental and non-fundamental power sharing among PVs using three different control strategies are presented in Figure 12. As can be seen, all three control strategies have acceptable results in terms of the fundamental active and reactive power sharing. Although the non-fundamental power in the decentralized control strategy is not aligned with the rated power of the PVs, both the central secondary control and the proposed distributed secondary control strategies effectively share it among the PVs. According to the differences in the discussed control strategies, the weakness of the decentralized control strategy [22] in non-fundamental power sharing can be explained by not using virtual impedance in the path of harmonic currents. It should be noted that in [5], only virtual resistance was used to improve non-fundamental power sharing. While in the virtual impedance structure presented in this paper, measures are also considered to reduce circulating currents between PVs and prevent resonance.

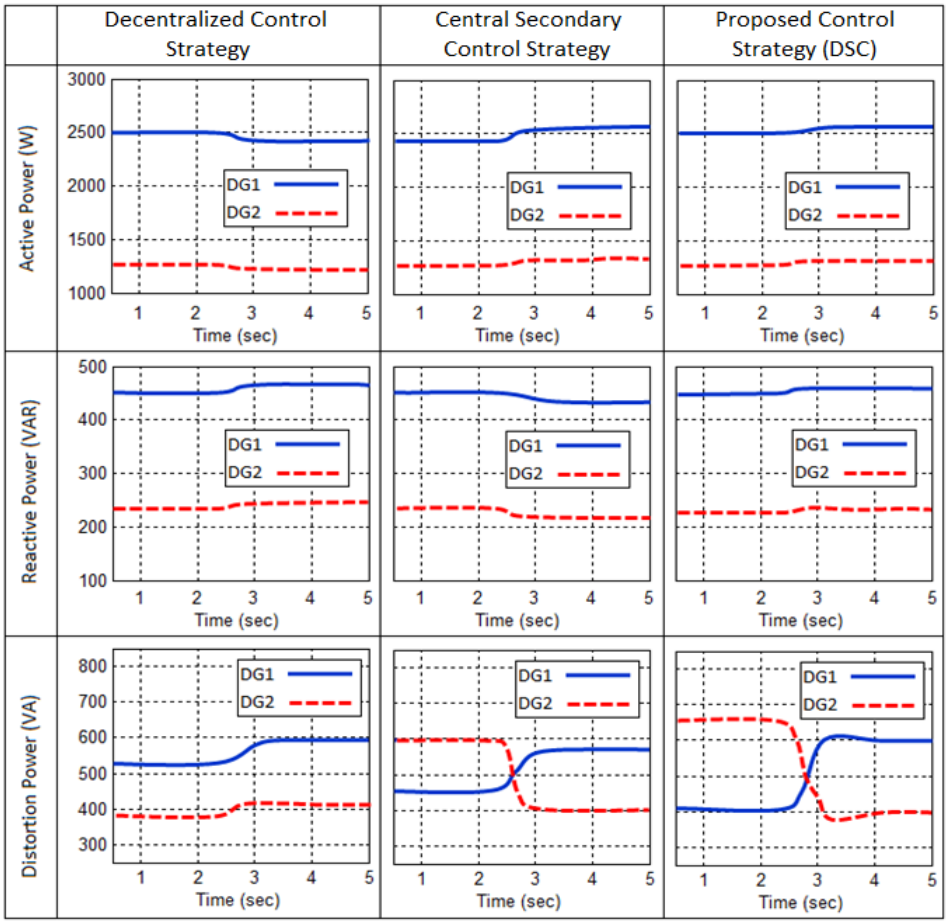

Figure 12. Fundamental and non-fundamental powers sharing among PVs.

Based on the simulation results from the first and second steps, Figure 13 shows the voltage harmonic indices before and after harmonics compensation. The previous sections discuss how VHIs can be used to increase the accuracy of non-fundamental power sharing, which can lead to increased voltage distortion at the output of PVs. As shown in Figure 13, in the decentralized control strategy, the output voltage of the PVs without the use of VHI is now significantly disturbed. In the decentralized control strategy, disturbances in the output voltage of the PVs (in step 1) are generated by controlling the PV output voltage across the harmonic spectrum using a PI controller. Meanwhile, in the proposed control strategy and central secondary control strategy, the output voltage of PVs (in step 1) has negligible THD. In the proposed strategy, separate resonance controllers are used to control voltage and current harmonics. These controllers work to maintain a sinusoidal output voltage of the PVs. This can be seen in Figure 13, where the output voltage of PVs shows small values of THD.

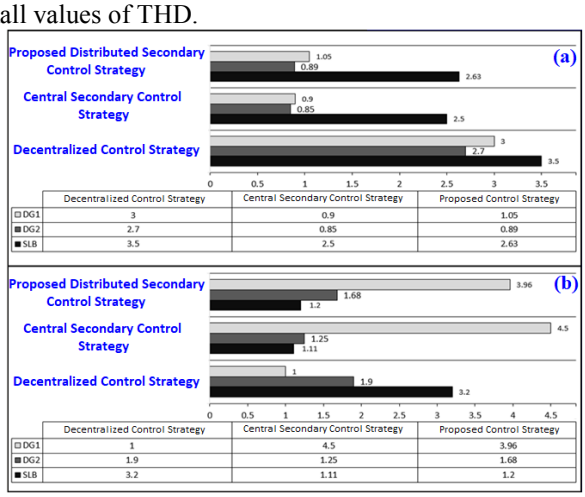

Figure 13. Comparison of voltage THD in different Strategies (%) before (a) and after (b) compensation.

Figure 13 shows that in the second step of the simulation, even after applying the voltage harmonic compensation in the decentralized control strategy, there are still significant harmonics in the SLB voltage. In contrast, both the proposed control strategy and the central secondary control strategy successfully minimize the voltage THD in the SLB. The proposed control strategy includes separately distributed voltage and frequency restoration units on the secondary control level of PVs to recover MG voltage and frequency. Comparing the numerical results in Figure 14 shows that the proposed strategy effectively limits the MG voltage and frequency deviation.

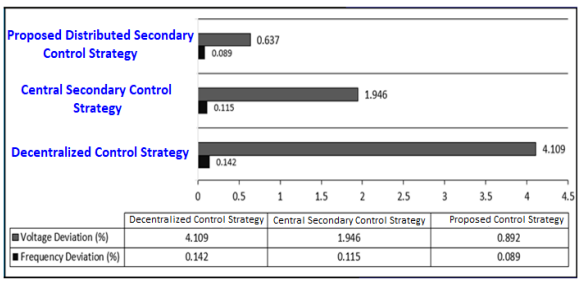

	Decentralized Control Strategy	Central Secondary Control Strategy	Proposed Control Strategy
Voltage Deviation (%)	4.109	1.946	0.892
Frequency Deviation (%)	0.142	0.115	0.089

Figure 14. Comparison of voltage and frequency deviation in different control strategies (%).

5. Conclusions and future work

In this paper, a distributed control strategy is proposed to improve power quality in PV-based IMGs. In the proposed control scheme which is based on the local control of PVs, each PV has a primary control level and a secondary control level. Unlike the central secondary control strategy, both primary and secondary controllers are implemented locally. In this structure, there is no central secondary control system and therefore there is no need for communication links between the primary and secondary control levels. Therefore, the proposed control strategy has higher reliability than centralized secondary control. In the proposed strategy, the secondary controller directs the compensation by sending reference signals to the primary controllers. Also, a method for SLB voltage harmonic compensation was proposed, which takes into account the available capacities of the PV interface inverters in the compensation and stops the compensation if there is not enough capacity to avoid overload. It was shown that the proposed strategy is capable of compensating SLB voltage harmonics without the need of distribution line information. The influence of the proposed control on the output voltage quality of the PVs is neglectable, and this is because the compensation loops are located in the circulating current paths of the harmonic components rather than in the current paths of linear and non-linear MG loads. The simulation results are presented in several different steps and different aspects of the control system performance are evaluated separately. The simulation results show the appropriate sharing of fundamental and non-fundamental powers among PVs based on their rated capacity and free capacity. Also, the proposed voltage and frequency controllers in the secondary control levels effectively minimize the voltage and frequency deviation, while compensating the voltage harmonics in the SLB. Comparison of simulation results with centralized secondary control and decentralized control strategies has confirmed the effectiveness of the proposed distributed control strategy in improving the power quality and reliability of PV-based islanded MGs.

Looking ahead, there are several topics that hold promise for future work:

- The proposed distributed secondary control approach can be developed for seamless transition control between islanded and grid-connected modes.
- The proposed method for harmonic compensation workload sharing between PVs can be developed specifically for scenarios involving active harmonic filters in MG.
- The proposed strategy for compensating IMG voltage harmonics can be developed for effective operation in both islanded and grid-connected configurations.

Nomenclature

p	PV output instantaneous active power
$\bar{p}$	PV output fundamental active power
$\tilde{p}$	PV output non-fundamental active power
q	PV output instantaneous reactive power
$\bar{q}$	PV output fundamental reactive power
$\tilde{q}$	PV output non-fundamental reactive power
ϕ^*	PV outpot phase angle reference
E^*	PV outpot voltage amplitude reference
ϕ_0	PV outpot rated phase angle
E_0	PV outpot rated voltage amplitude
ω_0	PV outpot fundamental frequency
m_p	proportional coefficients of active power controllers
m_i	integral coefficients of active power controllers
n_p	proportional coefficient of reactive power

	controllers
K_{pV}	PR voltage controllers proportional coefficient
K_{pI}	PR current controllers proportional coefficient
K_{rVh}	PR voltage controllers resonant coefficient in h^{th} harmonic order
K_{rIh}	PR current controllers resonant coefficient in h^{th} harmonic order
ω_{cV}	PR voltage controllers cut-off frequency
ω_{cI}	PR current controllers cut-off frequency
R_v^1	Virtual fundamental resistance
R_v^h	Virtual harmonic (h^{th}) resistance
L_v^1	Virtual fundamental inductance
L_v^h	Virtual harmonic (h^{th}) inductance
$\delta\omega_{PVk}$	Frequency restoration signal of PV$_k$ in every sample time
δE_{PVk}	Voltage restoration signal of PV$_k$ in every sample time
$\bar{\omega}_{PVk}$	Frequency average for all PV units
$\bar{E}_{PVk}$	Voltage average for all PV units
HD_{SLB}^h	Voltage harmonic (h^{th}) distortion index in SLB
$C_{dq,k}^h$	Voltage harmonic (h^{th}) compensation reference of PV$_k$
S_0	PV inverter rated capacity
S_r	PV inverter available capacity for supplying non-fundamental power
S_{fr}	PV inverter remaining capacity after supplying non-fundamental power
$G_{cl}(s)$	PV control system closed-loop transfer function
$Z_o(s)$	Equivalent output impedance of the closed-loop system
$Z_v(s)$	Virtual impedance in closed-loop system
$Z_o'(s)$	PV inverter output impedance

References

[1] Wang, Y., Tang, J., Si, J., Xiao, X., Zhou, P., Zhao. J. (2023). Power quality enhancement in islanded microgrids via closed-loop adaptive virtual impedance control. Protection and Control of Modern Power Systems, 8(10), 1-17.
https://doi.org/10.1186/s41601-023-00284-z.

[2] Lingampalli, B. R., Kotamraju, S. R., (2022). Analysis of passive islanding detection techniques for double line fault in three phase microgrid system. *Advances in Electrical and Electronic Engineering*, 20(2), 115-130.
https://doi.org/10.15598/aeee.v20i2.4300.

[3] Li, S., Oshnoei, A., Blaabjerg, F., Anvari-Moghaddam, A., (2023). Hierarchical Control for Microgrids: A Survey on Classical and Machine Learning-Based Methods. *Sustainability*, 15(11), 1-22. https://doi.org/10.3390/su15118952.

[4] Alonsoa, A. M. S., Brandaoc, D. I., Caldognettod, T., Marafaoa, F. P., Mattavelli, P., (2020). A selective harmonic compensation and power control approach exploiting distributed electronic converters in microgrids. *International Journal of Electrical Power and Energy Systems*, 115(1), 1-15.
https://doi.org/10.1016/j.ijepes.2019.105452.

[5] Savaghebi, M., Jalilian, A., Vasquez, J. C., Guerrero, JM., (2012). Secondary control for voltage quality enhancement in microgrids," *IEEE Transactions on Smart Grid*, 3(4), 1893-1902. https://doi.org/10.1109/TSG.2012.2205281.

[6] Savaghebi, M., Jalilian, A., Vasquez, J. C., Guerrero, JM., (2012). Secondary control scheme for voltage unbalance compensation in an islanded droop-controlled microgrid. *IEEE Transactions on Smart Grid*, 3(2), 797-807. https://doi.org/10.1109/TSG.2011.2181432.

[7] Savaghebi, M., Vasquez, J. C., Jalilian, A., Guerrero, JM., (2013). Selective compensation of Voltage harmonics in grid-connected microgrids. *International Journal of Mathematics and Computers in Simulation*, 91(1), 211-228. https://doi.org/10.1016/j.matcom.2012.05.015.

[8] Fani B., Zandi, F., Karami-Horestani, A., (2018). An enhanced decentralized reactive power sharing strategy for inverter-based microgrid. *International Journal of Electrical Power and Energy Systems*, 98(1), 531-542.
https://dx.doi.org/10.1016/j.ijepes.2017.12.023.

[9] Golsorkhi, M. S., Lu, D. D., Guerrero, J. M., (2017). A GPS-based decentralized control method for islanded microgrids. *IEEE Transactions on Power Electronics*, 32(2), 1615-1625.
https://dx.doi.org/10.1109/TPEL.2016.2551265.

[10] Mousavi, S.Y.M., Jalilian, A., Savaghebi, M., Guerrero, J.M., (2018). Autonomous control of current and voltage controlled DG interface inverters for reactive power sharing and harmonics compensation in islanded microgrids. *IEEE Transactions on Power Electronics*, 33(11), 9375-86. https://dx.doi.org/10.1109/TPEL.2018.2792780.

[11] Zhang, Z., Gao, S., Zhong, C., Zhang, Z., Rodríguez, F. J., (2023). Accurate Active and Reactive Power Sharing Based on a Modified Droop Control Method for Islanded Microgrids. *Sensors*, 23(14), 1-22. https://doi.org/10.3390/s23146269.

[12] Farokhian-Firuzi, M., Roosta, A., Gitizadeh, M., (2019). Stability analysis and decentralized control of

inverter-based ac microgrid. *Protection and Control of Modern Power System*, 4(1), 1-24. https://dx.doi.org/10.1186/s41601019-0120-x.

[13] Rashwan, A., Mikhaylov, A., Senjyu, T., Eslami, M., Hemeida, A.M., Osheba, D.S.M, (2023). Modified Droop Control for Microgrid Power-Sharing Stability Improvement. *Sustainability*, 15(14), 11220. https://doi.org/10.3390/su151411220.

[14] Wang, H., Zeng, G., Dai, Y., (2021). Research on modified droop control of distributed generation units by adaptive population-based external optimization. *Power System Protection and Control*, 45(7), 2483–2491.

[15] Chen, H., Tang, Z., Lu, J., et al. (2021). Research on optimal dispatch of a microgrid based on CVaR quantitative uncertainty. *Power System Protection and Control*, 49(5), 105–115.

[16] Sahoo, B., Alhaider, M. M., Rout, P. K., (2023). Power quality and stability improvement of microgrid through shunt active filter control application: An overview. *Renewable Energy Focus*, 44(1), 139-173. https://doi.org/10.1016/j.ref.2022.12.006.

[17] Wang, X., Blaabjerg, F., Chen, Z., (2014). Autonomous control of inverter-interfaced Distributed Generation units for harmonic current iltering and resonance damping in an islanded micro-grid. *IEEE Transactions on Industry Applications*, 50(1), 452-461. https://doi.org/10.1109/TIA.2013.2268734.

[18] Hosseinpour, M., Kholousi, A., (2023). Design and Analysis of LCL-type Grid-Connected PV Power Conditioning System Based on Positive Virtual Impedance Capacitor-Current Feedback Active Damping. *Journal of Solar Energy Research*, 8(2), 1497-1515. https://doi.org/10.22059/jser.2023.357089.1286

[19] Zhou, J., et al. (2018). Consensus-based distributed control for accurate reactive, harmonic and imbalance power sharing in microgrids. *IEEE Transactions on Smart Grid*, 9(4), 2453–2467. https://doi.org/10.1109/TSG.2016.2613143.

[20] Gao, Y., Ai, Q., (2018). Distributed cooperative optimal control architecture for AC microgrid with renewable generation and storage. *International Journal of Electrical Power and Energy Systems*, 96(1), 324-334. https://doi.org/10.1016/j.ijepes.2017.10.007.

[21] Sreekumar, P., Khadkikar, V., (2017). Direct control of the inverter impedance to achieve controllable harmonic sharing in the islanded microgrid. *IEEE Transactions on Industrial Electronics*, 64(1), 827–837. https://doi.org/10.1109/TIE.2016.2574308.

[22] Guerrero, J. M., Matas, J., Vicuña, L. G., Castilla, M., Miret, J., (2017). Decentralized Control for Parallel Operation of Distributed Generation Inverters Using Resistive Output Impedance. *IEEE Transaction on Industrial Electronics*, 54(2), 994-1004. https://doi.org/10.1109/TIE.2007.892621.

[23] Shafiee, Q., Guerrero, J. M., Vasquez, J. C., (2014). Distributed Secondary Control for Islanded Microgrids-A Novel Approach. *IEEE Transaction on Power Electronics*, 29(2), 1018-1031. https://doi.org/10.1109/TPEL.2013.2259506.

[24] Lian, Z., Wen, C., Guo, F., Lin, P., Wu, Q., (2023). Decentralized secondary control for frequency restoration and power allocation in islanded AC microgrids. *International Journal of Electrical Power and Energy Systems*, 148(1), 1-9. https://doi.org/10.1016/j.ijepes.2022.108927.

[25] Sai Thrinath, B. V., Venkata Ramana, C., Meghya Nayak, B., Yashashwini, B., Kumar, N. M., Ezhilvannan, P., (2023). An Uninterrupted Fuzzy-Based PV-BES System for Improving Power Quality in Grid Connected Systems. *Journal of Solar Energy Research,* 8(3), 1622-1634. https://doi.org/10.22059/jser.2023.359127.1304

[26] Xin, H., Zhang, L., Wang, Z., Gan, D., Wong, K. P., (2015). Control of Island AC Microgrids Using a Fully Distributed Approach. *IEEE Transactions on Smart Grid*, 6(2), 943–945. https://doi.org/10.1109/TSG.2014.2378694.

[27] Ibacache, R. P., Yazdani, A., Silva, C., Agüero, J. C., (2019). Decentralized Unified Control for Inverter-Based AC Microgrids Subject to Voltage Constraints. *IEEE Access*, 7(1), 157318-157329. https://doi.org/10.1109/ACCESS.2019.2944898.

[28] Gu, W., Lou, G., Tan, W., Yuan, X., (2017). A nonlinear state estimator-based decentralized secondary voltage control scheme for autonomous microgrids. *IEEE Transactions on Smart Grid*, 32(6), 4794-804. https://doi.org/10.1109/TPWRS.2017.2676181.

[29] Khayat, Y., Naderi, M., Shafiee, Q., Batmani, Y., Fathi, M., Guerrero, JM., Bevrani, H., (2019). Decentralized optimal frequency control in autonomous microgrids. *IEEE Transaction on Power Systems*, 34(3), 2345-2353. https://doi.org/10.1109/TPWRS.2018.2889671.

[30] Vasquez, JC., Guerrero, JM., Savaghebi, M.,

Carrasco, E. G., Teodorescu, R., (2013). Modeling, Analysis, and Design of Stationary Reference Frame Droop Controlled Parallel Three-Phase Voltage Source Inverters. *IEEE Transaction on Industrial Electronics*, 60(4), 1271-1280. https://doi.org/10.1109/TIE.2012.2194951.

[31] Mohammadzadeh, M., Ketabi, A., (2021). Single and Three Phases Sensitive Load Compensation by Electric Spring Using Proportional-Resonant and Repetitive Controllers. *Journal of Solar Energy Research*, 6(2), 713-725. https://doi.org/10.22059/JSER.2021.317583.1190

[32] IEEE Standard 1459 (2010). IEEE Standard Definitions for the Measurement of Electric Power Quantities under Sinusoidal, Non-sinusoidal, Balanced, or Unbalanced Conditions. https://doi.org/10.1109/IEEESTD.2010.5439063.